Available online at www.sciencedirect.com
ScienceDirect
Journal of the European Ceramic Society 29 (2009) 3341–3348
www.elsevier.com/locate/jeurceramsoc

Size effects on χ- to α-Al_2O_3 phase transformation

Pei-Ling Chang *, Yu-Chun Wu, Ssu-Jung Lai, Fu-Su Yen [1]

Department of Resources Engineering, National Cheng Kung University, No. 1 University Rd., Tainan 70101, Taiwan

Received 4 February 2009; received in revised form 24 June 2009; accepted 1 July 2009
Available online 28 July 2009

Abstract

Nano-scaled χ-Al_2O_3 powders with d_{50} mean particle sizes from 17 to 314 nm were prepared to investigate the size effect on their phase transformation. Structural properties and crystallization behavior as a function of thermal treatments of various-sized χ-Al_2O_3 particles were examined by DTA, XRD and TEM characterizations. It was confirmed that the decrease of particle size allows for stable α-Al_2O_3 formation at relatively low temperature. Furthermore, the phase transformation route of χ-Al_2O_3 to α-Al_2O_3 was also modified due to the decrease of particle size. A critical size of χ-Al_2O_3 that determines the phase transformation behavior was found to be around 40 nm. For particles larger than 40 nm, a transition phase of κ-Al_2O_3 is formed before obtaining final α-Al_2O_3 phase. Nevertheless, for those smaller than the critical size, starting χ-Al_2O_3 particles have to grow to 40 nm and then directly transform to α-Al_2O_3 bypassing κ-Al_2O_3 at a temperature as low as 1050 °C.

Keywords: Al_2O_3; Calcination; Phase transformation; Particle size; Activation energy

1. Introduction

It is well-known that the particle size has obvious effects on material properties. In particular, the stability of crystal phase has been found to be modified by the crystallite size in various material systems when their sizes nano-scaled. For example, TiO_2 nanocrystallites show a polymorphous reversibility between anatase and rutile when the crystallite size is around 14.5 nm.[1,2] The stable phase of $BaTiO_3$ crystallites at room temperature becomes cubic instead of tetragonal when their size is reduced to 30 nm.[3] Similar cases have also been observed in which *cubic*-$PbTiO_3$ and *tetragonal*-ZrO_2 crystallites may exist at room temperature in place of *tetragonal*-$PbTiO_3$ and *monoclinic*-ZrO_2 crystallites, respectively, when the crystallite size is smaller than a few nanometers.[4–6] The specific size that leads to variations in crystallization behavior as described above is called "critical size". From the viewpoint of nucleation-growth mechanism, to reach such "critical size" is necessary in order to conduct a system from metastable condition to thermodynamically stable phase.[7,8] In the case of typical θ-Al_2O_3 → α-Al_2O_3 transformation route, stable α-Al_2O_3 cannot be obtained unless the θ-Al_2O_3 precursor has grown up to the critical size of 20–25 nm.[9,10] Similarly, anatase TiO_2 crystallite has to be also larger than 10 nm to lead to a transformation to rutile phase.[2,11]

Size effect has been reported to modify the phase transformation path of gibbsite ($Al(OH)_3$) where two routes may undergo:[12,13]

gibbsite → χ-Al_2O_3 → κ-Al_2O_3 → α-Al_2O_3(route1)

↘ boehmite → γ-Al_2O_3 → δ-Al_2O_3 → θ-Al_2O_3
→ α-Al_2O_3(route2)

For micrometric particles, both transition routes may occur depending on synthetic conditions. However, phase transformation mainly follows route 1 when the particle size is smaller than 1 μm.[12,13] It has been reported that α-Al_2O_3 can be obtained directly from χ-Al_2O_3 bypassing intermediate κ-Al_2O_3 phase when its particle size is as small as 10 nm.[14–16] In addition, a phase transformation bypassing transition phases has also been observed for ultrafine Al_2O_3 powder treated by mechanical grinding techniques.[17–19] Therefore, it is believed that a new transition path of χ-Al_2O_3 → α-Al_2O_3 should exist under a certain critical condition, in particular a certain critical size.

In order to investigate size effect on the phase transformation of χ-Al_2O_3 to α-Al_2O_3, starting χ-Al_2O_3 with various particle

* Corresponding author. Tel.: +886 6 2381001; fax: +886 6 2380421.
E-mail addresses: chang620@gmail.com (P.-L. Chang), yfs42041@mail.ncku.edu.tw (F.-S. Yen).
[1] Tel.: +886 6 2355603; fax: +886 6 2380421.

0955-2219/$ – see front matter © 2009 Elsevier Ltd. All rights reserved.
doi:10.1016/j.jeurceramsoc.2009.07.002

Table 1
Basic properties of the examined χ-Al_2O_3 samples.

Sample name	Cn	Cf	C155	C65	C55	C40	C22	C19	C17
d_{50} (nm)	314	72	155	65	55	40	22	19	17
d_{90} (nm)	596	340	310	121	104	70	41	34	34

Cn: as-calcined and Cf: as-fragmented.

sizes ranging from 17 to 155 nm were prepared with fragment treatment. Classification was carried out used the centrifuge technique. Moreover, this study examined structural properties and quantitative analysis of the phase composition as a function of heat treatment. Activation energy and mechanisms of crystallization for α-alumina formation related to a particle size will be presented and discussed.

2. Experimental details

2.1. Sample preparation

Starting χ-Al_2O_3 particles were obtained by heat treating commercial gibbsite powder (S11, Almatis Inc., d_{50} = 0.25–0.31 μm) at 600 °C for 30 min with a heating rate of 2 °C/min. Aqueous slurries containing 30 wt% of χ-Al_2O_3 were prepared for the fragment treatment by the Perl mill apparatus (Drais, PML-H/V). The samples with and without fragment treatment are labeled as Cf and Cn, respectively. Classification of the Cf sample was then carried out by centrifuge technique to obtain various sizes of χ-Al_2O_3 for the following studies. Seven samples with different particle sizes were labeled C155, C65, C55, C40, C22, C19 and C17 denoted by their d_{50} sizes, i.e. 155, 65, 55, 40, 22, 19 and 17 nm, respectively. The d_{50} and d_{90} particles sizes of all the prepared samples are summarized in Table 1.

The samples Cn, C155, C40 and C17 were selected for the observation of phase transformation. Their particle size distributions (PSD) as measured by a dynamic light scattering spectroscopy (Malvern Zetasizer 1000) are shown in Fig. 1. It is apparent that the fragmented samples generally exhibit normal size distribution. The morphology of these samples was carried out by transmission electron microscope (TEM, Hitachi HF-2000) as presented in Fig. 2. It is shown in Fig. 2(a) that the starting χ-Al_2O_3 particles before fragment treatment are platelet-like on the (0 0 1) plane with a pseudo-hexagon external form of the originate gibbsite.[12,20] The platelet-like morphology was gradually destroyed by fragment treatment and is less obvious when the particles are smaller as illustrated in Fig. 2(b)–(d). The selected-area electron diffraction (SAED) patterns shown in the inset of Fig. 2 also confirms that the fragment treatment indeed results in the disfiguration of preferred orientation on the (0 0 1) plane. These samples were then thermal treated with a heating rate of 10 °C/min at scheduled temperatures from 900 to 1500 °C and quenched to room temperature immediately.

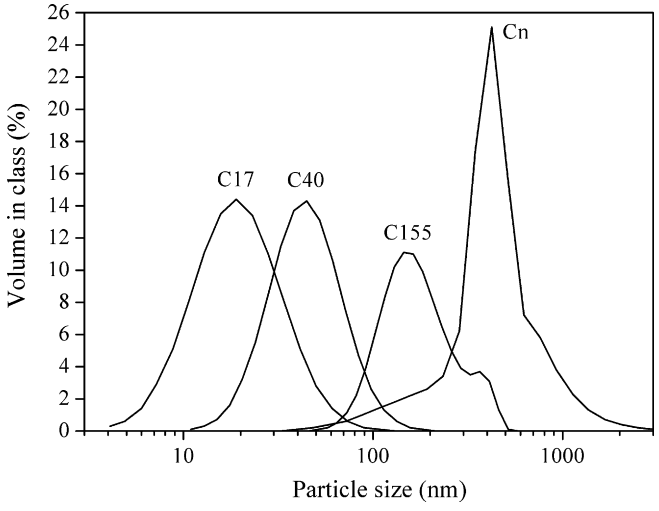

Fig. 1. Particle size distributions of Cn, C155 (d_{50} = 155 nm), C40 (40 nm) and C17 (17 nm) samples before heat treatments.

Thermal behavior was examined by differential thermal analysis (DTA, Setaram TGA92) at a heating rate of 10 °C/min up to 1500 °C. The crystalline phase was identified by powder X-ray diffraction (XRD, Rigaku MiniFlex,) using Cu Kα radiation scanning from 10° to 80° (2θ) with a scanning rate of 4°/min. Quantitative analysis of κ- and α-Al_2O_3 phase composition was undertaken by XRD powder method by adding 10 wt% of CaF_2 as a internal standard in the measuring samples. XRD measurement ranging from 24° to 38° with a scanning rate of 0.5°/min was performed for the determination of integrated intensities of κ-Al_2O_3 (0 1 3), α-Al_2O_3 (0 1 2) and CaF_2 (1 1 1) diffraction peaks. In order to establish calibration lines for the quantitative analysis of phase composition, heat treatments to the S11 gibbsite were undertaken at 1200 and 1500 °C with a heating rate of 2 °C/min to obtain pure κ-Al_2O_3 and α-Al_2O_3, respectively. Various weight ratios of κ-Al_2O_3/χ-Al_2O_3 and α-Al_2O_3/χ-Al_2O_3 with 10 wt% of CaF_2 were prepared as calibration samples. The calibration lines of κ-Al_2O_3 and α-Al_2O_3 were established by measuring the intensity ratios of κ-Al_2O_3/CaF_2 and α-Al_2O_3/CaF_2 peaks of the calibration samples, respectively. The fraction of χ-Al_2O_3 was obtained by deducting the sum of κ-Al_2O_3 and α-Al_2O_3 from the total. Data calculations were assisted by XRD Pattern Processing and Identification software (Jade 5.0, Material Data Inc.). The mean crystallite size of α-Al_2O_3 was determined by the Scherrer formula [21] using (0 1 2) diffraction peak correcting the instrument peak width obtained from the peak (1 1 1) of well-crystallized silicon powder. The morphology of final α-Al_2O_3 crystallite was carried out by TEM (FEI, Tecnai F20 G2). The activation energy of α-Al_2O_3 formation was evaluated by isothermal experiments according to the Arrhenius method.[22] Samples were isothermally treated in a platinum crucible at temperatures between 1025 and 1290 °C for various durations up to 60 min. The phase fraction was determined by the same method as the quantitative analysis as described above.

3. Results and discussion

3.1. The phase transformation of χ-Al_2O_3

XRD patterns of Cn, C155, C40 and C17 heating at various temperatures are shown in Fig. 3. It is observed that all the

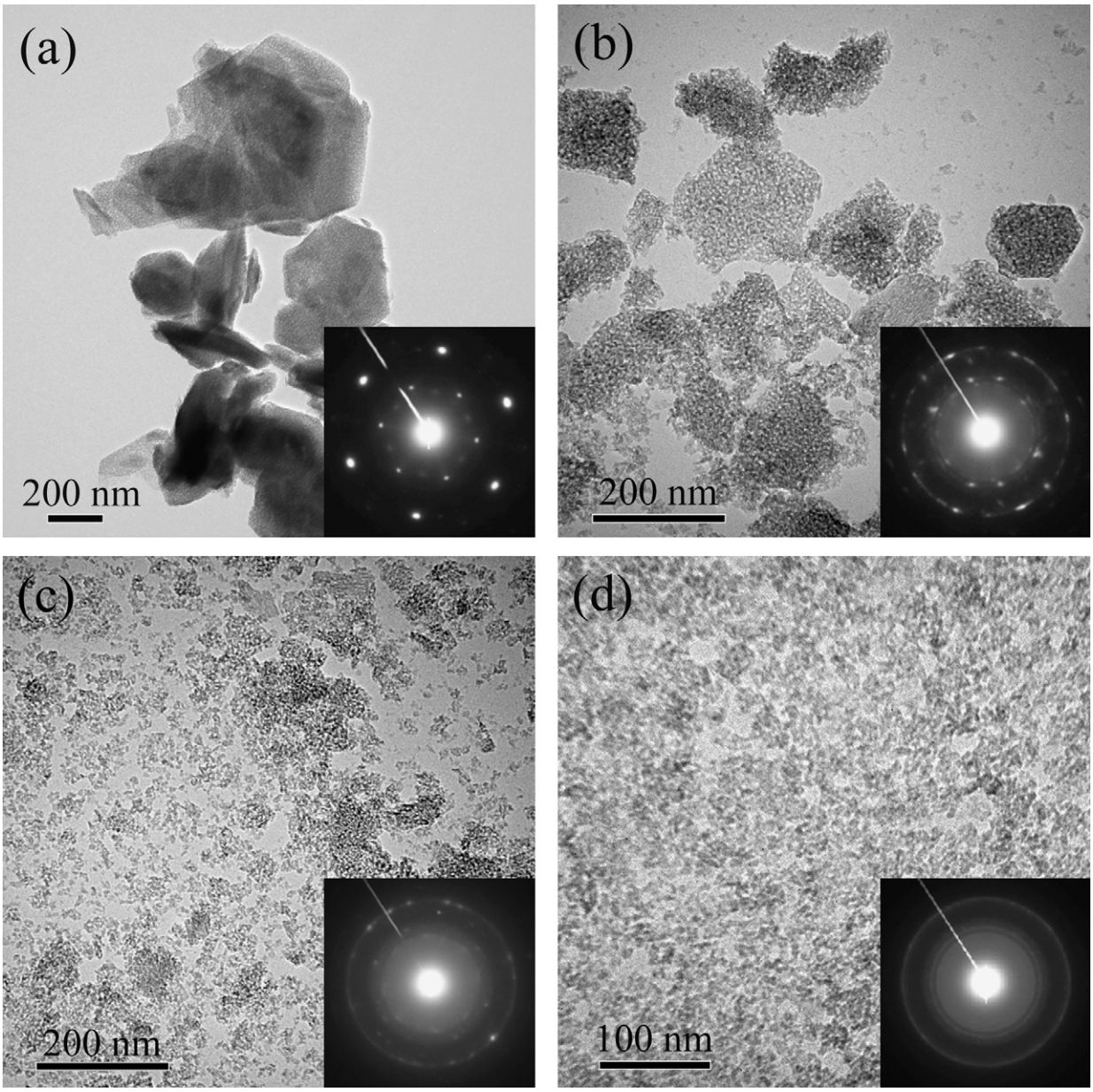

Fig. 2. TEM micrographs with SAED patterns of χ-Al_2O_3 samples (a) Cn (as calcined), size classified samples (b) C155, (c) C40 and (d) C17.

samples exhibit similar XRD patterns as heated at 900 °C. The first appearance of α-Al_2O_3 occurs at 1300 °C for Cn and is down to 1050 °C for C40 and C17. However, the formation of κ-Al_2O_3 takes place at higher temperature and shows a more indistinct peak when the particles size is smaller. Moreover, the existing range of κ-Al_2O_3 is between 1000 and 1350 °C for Cn and is obviously narrowed to 1050–1150 °C for C17.

Phase compositions of Cn, C155, C40 and C17 samples according to quantitative analyses associated with their DTA curves are shown in Fig. 4. For the Cn sample, an obvious exothermal peak emerges at around 950–1150 °C corresponding to a decrease of χ-Al_2O_3 along with an increase of κ-Al_2O_3. This exothermal peak can thus be assigned to the phase transformation $\chi \rightarrow \kappa$-Al_2O_3 [as marked (I) in the figure]. A second exothermal peak appears at around 1250–1400 °C which contributes to the phase transformation of $\kappa \rightarrow \alpha$-$Al_2O_3$ [as marked (II) in the figure]. For sample C155, the reaction (I) shifts to a higher temperature while reaction (II) shifts downward to a lower temperature in comparison with what occurred for the Cn sample. For sample C40, α-Al_2O_3 is found to coexist with κ-Al_2O_3 at 1050 °C indicating that a direct phase transformation from $\chi \rightarrow \alpha$-Al_2O_3 may take place [as marked (III) in the figure]. In its associated DTA curve, a very slight exothermic peak is observed at around 1150–1250 °C which is assigned to the $\kappa \rightarrow \alpha$-$Al_2O_3$ transformation since κ-Al_2O_3 starts to decreases with a simultaneous increase of α-Al_2O_3 in this period while χ-Al_2O_3 always remains less than 10%. For sample C17, the quantity of κ-Al_2O_3 always remains less than 15% in all the heating ranges implying that the direct transformation $\chi \rightarrow \alpha$-Al_2O_3 becomes dominant, resulting in an apparent exothermal peak located at around 1150 °C. The experimental results discussed above confirm that the phase transformation of $\chi \rightarrow \alpha$-Al_2O_3

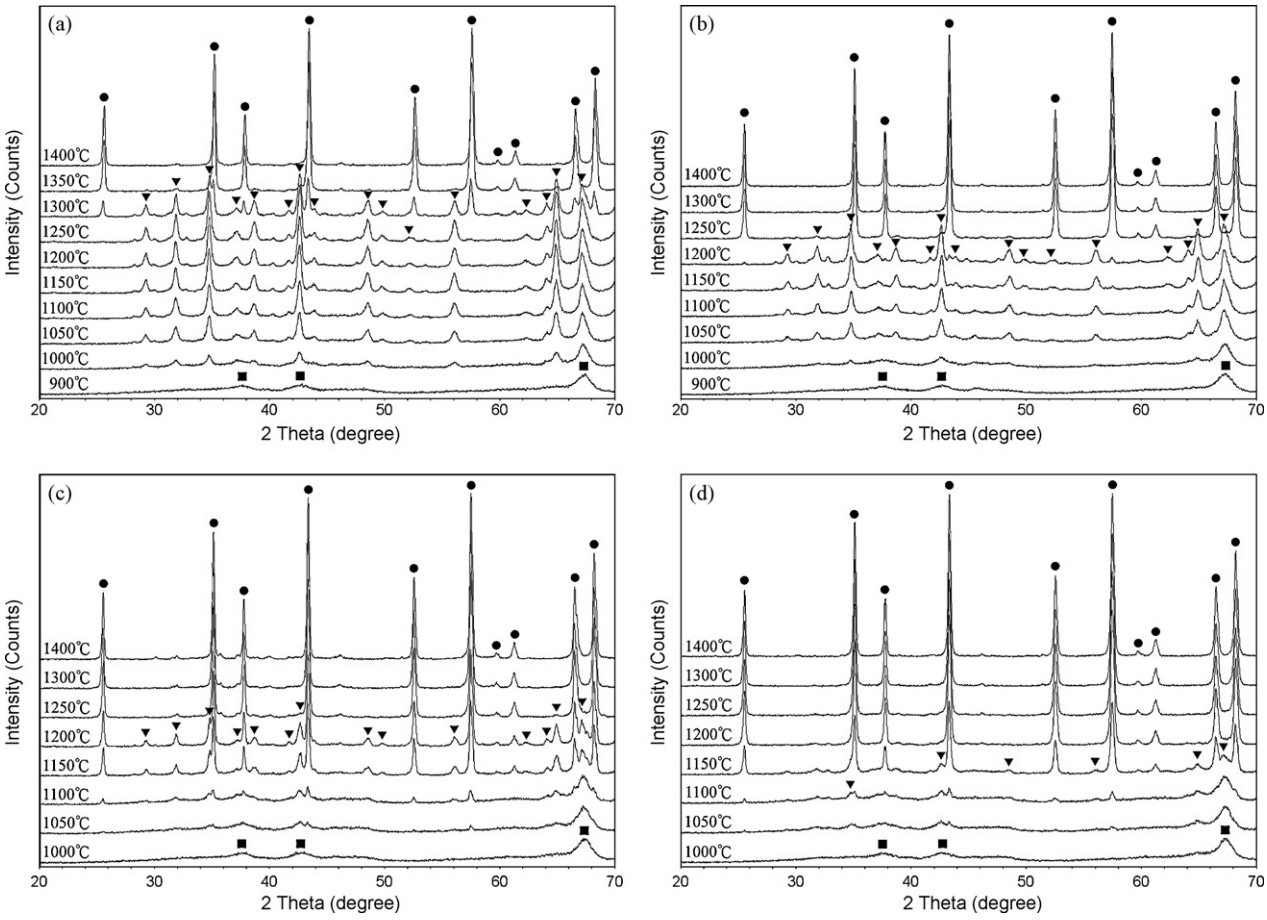

Fig. 3. XRD patterns of (a) Cn (as-calcined), (b) C155, (c) C40 and (d) C17 annealing at various temperatures of 900–1400 °C with heating rate of 10 °C/min and quenched to room temperature immediately. (●) α-Al_2O_3; (▼) κ-Al_2O_3; (■) χ-Al_2O_3.

depends on the particles size. For the large particles, the χ-Al_2O_3 is preferably transformed to κ-Al_2O_3 which turns to a stable α-Al_2O_3 phase at a higher temperature. Nevertheless, the χ-Al_2O_3 also allows for direct transformation to α-Al_2O_3 without forming κ-Al_2O_3 when the particle is reduced to a certain small size. In order to investigate such critical size, this study carried out activation energy of χ → α-Al_2O_3 formation as a function of particle size. This will be discussed in the following section.

3.2. Activation energy and particle size

This study evaluated activation energy of α-Al_2O_3 formation through isothermal experiments according to the Arrhenius method:[22] First-of-all, the values of rate constant k were obtained by the Johnson–Mehl–Avrami (JMA) equation as expressed in Eq. (1):[22]

$$x = 1 - \exp(-kt)^n \quad (1)$$

where x is the phase fraction of α-Al_2O_3 at time t and n is the reaction exponent. The kinetic experiments for all the samples were performed at three different temperatures ranging from 1050 to 1290 °C for at least six different holding times in order to obtain different temperature-dependent rate constants (k). As the values of k obtained, the activation energy (E_a) can be thus deduced according to the well-known Arrhenius equation as expressed in Eq. (2):

$$k = A \exp\left(\frac{-E_a}{RT}\right) \quad (2)$$

where A is a constant, R is the gas constant ($\sim 8.314\,J\,K^{-1}\,mol^{-1}$) and T is the working temperature. The deduced activation energies of α-Al_2O_3 formation as a function of their particles sizes are presented in Fig. 5. It is found that the evolution of activation energy according to particle size can generally be divided into two parts by sample C40. In regard to particle sizes larger than 40 nm, the activation energy decreases with the decrease of particles size down to minimum for sample C40. Normally, reducing particle sizes allows for the increase of surface energy that should result in a decrease of activation energy. However, the activation energy for the as-calcined sample (Cn) is surprisingly lower than that of C155, C65 and C55. This means something related to the fragment treatments provided a stronger influence than the size effect. Particle shape could be one important factor. As mentioned in the previous section, particles larger than 40 nm all show an apparent quantity of κ-Al_2O_3 during the phase transformation process which means the transition χ → κ-Al_2O_3 is an unavoidable step. According to the observation made by Ollivier[23] in addition to the present case, κ-Al_2O_3

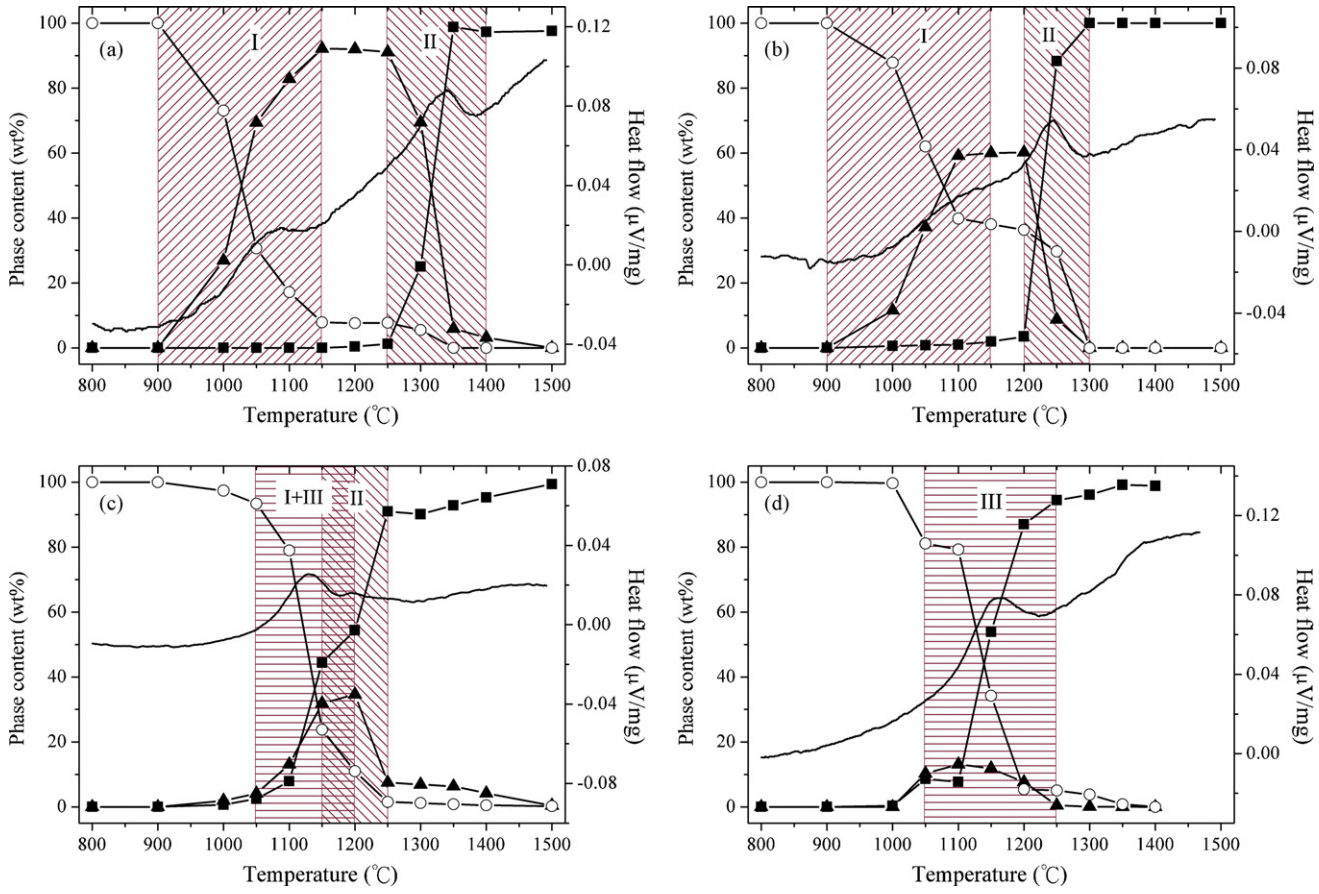

Fig. 4. Phase contents obtained at various temperatures of χ-Al_2O_3 samples (a) Cn (as-calcined), (b) C155, (c) C40 and (d) C17. The DTA curves are also inserted, and the reaction ranges are denoted as (I) χ → κ-Al_2O_3, (II) κ → α-Al_2O_3, (III) χ → α-Al_2O_3. (■) α-Al_2O_3; (▲) κ-Al_2O_3; (◯) χ-Al_2O_3.

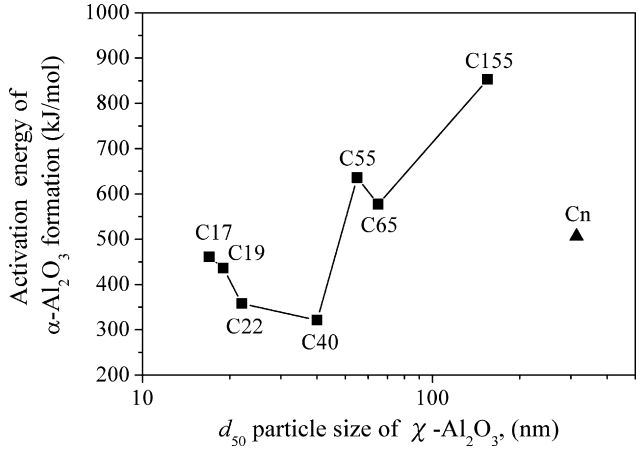

Fig. 5. Activation energy of α-Al_2O_3 formation as a function of the χ-Al_2O_3 size.

originating from gibbsite tends to exhibit a preferred orientation on the (0 0 1) plane and its plate-like morphology is similar to that of gibbsite.[13,24] The formation of κ-Al_2O_3 is supposed to be more favorable if it occurs on the (0 0 1) plane of χ-Al_2O_3 that leads to pseudomorphs as shown in Fig. 6(a) and (b). For the fragmented χ-Al_2O_3 particles, the surface proportion of the (0 0 1) plane to the overall surface areas is less distinct thus making the formation of κ-Al_2O_3 more difficult. In agreement with the observation shown in Fig. 6(a), κ-Al_2O_3 still keeps the original outline of χ-Al_2O_3 and shows a stack-layer appearance in parallel to the (0 0 1) plane. The shape effect may be the reason why the formation of κ-Al_2O_3 for C155 occurs at 1050 °C instead of at 1000 °C as for Cn. Moreover, the shape effect may also be the reason why the activation energy of C155 is higher than that of Cn This hypothesis is consistent with the mechanism of phase transformation interpreted by the Avrami exponent (n) as listed in Table 2. For C155, C65 and C55, the values of n are 1.07 and 0.85, which corresponds to a growth of isolated plates of finite size.[25] As the stack-layers

Table 2
Activation energy of α-Al_2O_3 formation of various-sized χ-Al_2O_3 samples.

Sample name	Cn	C155	C65	C55	C40	C22	C19	C17
E_a (kJ/mol)	506	853	577	636	321	358	436	461
n	1.49	1.07	0.85	0.85	1.38	1.44	1.36	1.51

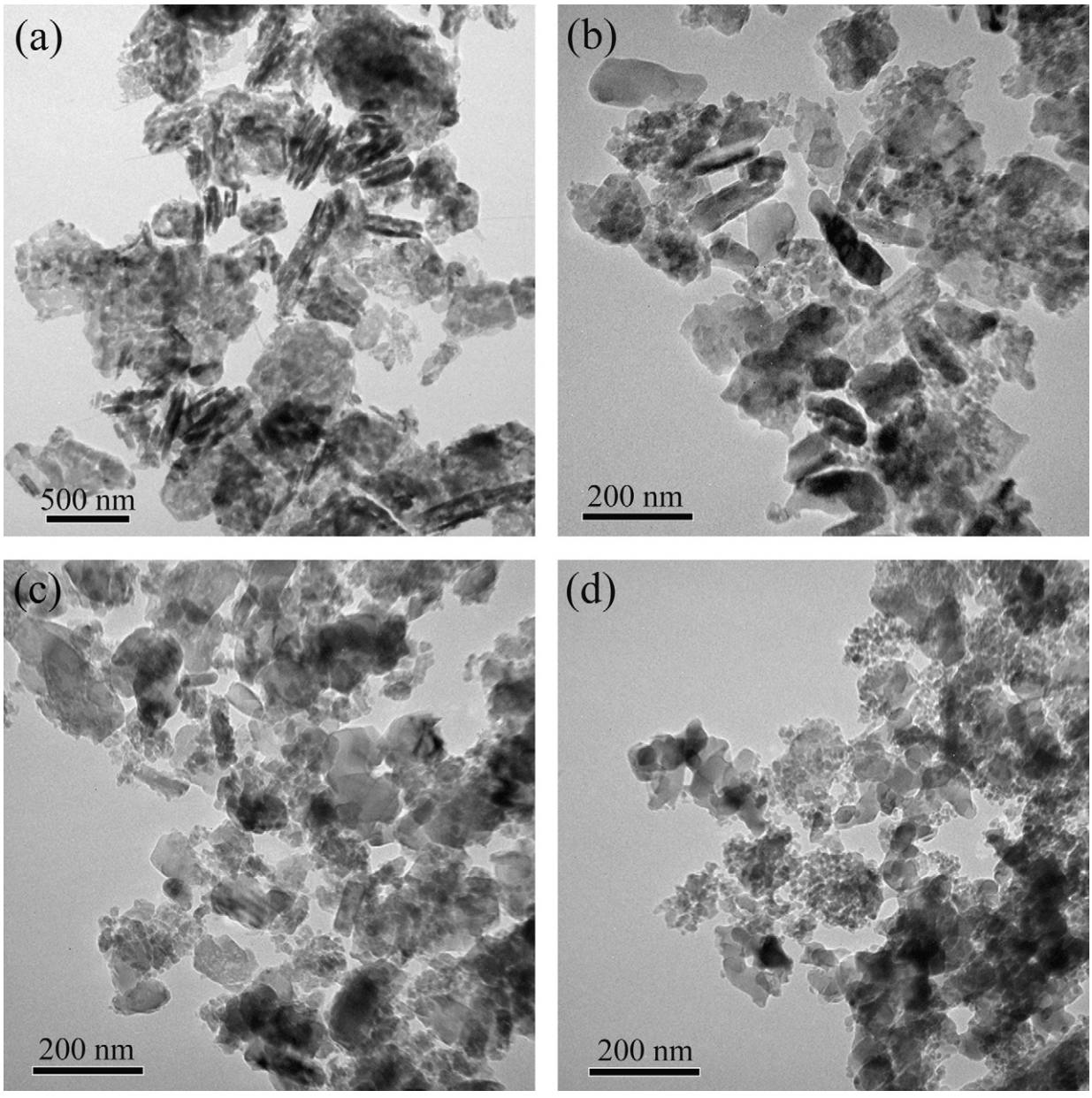

Fig. 6. TEM micrographs of (a) Cn and (b) C155 (c) C40 and (d) C17 annealed at 1150 °C. Phase composition of Cn: χ/κ = 8/92 (%), C155: χ/κ/α = 38/60/2 (%), C40: χ/κ/α = 24/32/44 (%), C17: χ/κ/α = 34/12/54 (%).

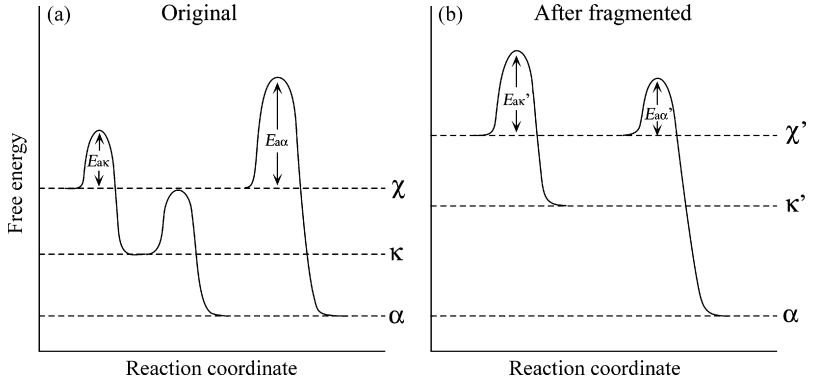

Fig. 7. Schematic representations of the Ostwald step rule of free energy for the $\chi \rightarrow \kappa \rightarrow \alpha$-$Al_2O_3$ phase transformations for the original (a) the after fragmented states (b). $E_{a\kappa}$ and $E_{a\alpha}$ denote the activation energies of $\chi \rightarrow \kappa$-Al_2O_3 ($E_{a\kappa}$) and $\chi \rightarrow \alpha$-Al_2O_3 ($E_{a\alpha}$), respectively. $E'_{a\kappa}$ and $E'_{a\alpha}$ represent the activation energies after fragment treatment.

are peeled off by fragment treatment, the plate particles are thus isolated as shown in Fig. 6(b) and (c). This indicates that the phase transformation of α-Al_2O_3 is indeed carried out by growth mechanism onto the isolated platelet-like κ-Al_2O_3. Since two-step phase transformation is necessary for the C155, C55 and C40 samples, the overall activation energy becomes a combination of the size and shape effects. Even through shape effect determines the formation of κ-Al_2O_3, the as-formed κ-Al_2O_3 is easier to transform to α-Al_2O_3 when the particle size is smaller. As a consequence, the overall activation energy decreases with particle size. Nevertheless, their activation energies are still higher than that of Cn in which the activation energy for χ → κ-Al_2O_3 should be very small (268 kJ/mol).

The activation energy increases again as the particles size becomes smaller than 40 nm. According to XRD and DTA characterization, the phase transformation for those samples is mainly carried out by the direct χ → α-Al_2O_3 transition route. For these samples, the platelet-like morphology is no longer present as illustrated in Fig. 6(d), proving that the shape factor is not effective anymore and can be neglected. As mentioned previously, reaching a critical size is an essential condition to induce phase transformation.[1,2,7–10] Particles smaller than 40 nm may have to grow to such a critical size to achieve phase transformation to α-phase. For those small particles (samples C40, C22, C19 and C17), their *n* values are all around 1.36–1.51, which is associated with the mechanism of the initial growth of particles nucleated at the start of transformation.[25] This indicates that an initial growth takes place at the early stage of phase transformation when the nucleation is still being processed. Additional energy is required to conduct crystal growth to around 40 nm, resulting in relatively higher activation energy for smaller particles.

Activation energy is related to the energy barriers of reactions which can be schematically represented by the Ostwald step rule as shown in Fig. 7. It is believed that the energy barrier for χ → κ-Al_2O_3 ($E_{a\kappa}$) is smaller than that of χ → α-Al_2O_3 ($E_{a\alpha}$) as illustrated in Fig. 7(a). Therefore, the later reaction is more difficult accomplish than the former under regular conditions. Generally, free energy increases with the decrease of particle size due to the strong surface-to-volume effect. The free energy of χ-Al_2O_3 increases when the particle reduces to nano-scale and finally causes the energy barrier of χ → α-Al_2O_3 ($E'_{a\alpha}$) to become smaller as depicted in Fig. 7(b). In the meantime, the energy barrier of χ → κ-Al_2O_3 ($E'_{a\kappa}$) increases with decreasing particle size due to the shape effect. The favorable transition route is thus a result of the competition between $E'_{a\kappa}$ and $E'_{a\alpha}$. Finally, χ → α-Al_2O_3 transition wins this competition and becomes dominant when the particle size is down to 40 nm. A similar crystallization behavior was also observed for the AIP derived χ-Al_2O_3 nanoparticle (primary particles ~10 nm) where no χ → κ-Al_2O_3 was observed during the phase transformation.[14–16] Evidently, is obvious that the phase transformation of the samples with size above and below 40 nm is performed by two different mechanisms. Accordingly, 40 nm is suggested as the critical size in the present system.

Wen and co-workers showed that the nucleation stage is maintained when the yield of α-Al_2O_3 is less than 5 wt% during θ → α-Al_2O_3 phase transformation and the apparent crystallite size in this nucleation stage can be denoted as the critical size.[9,10] The crystallite size is coarsened by the growth process at the as-formed nuclei. In order to further investigate the critical size for the present system, Fig. 8(a) presents the size of the α-Al_2O_3 particle for the samples C17, C19, C22, C33 and C40 as a function of its containing percentage. It is apparent that the α-Al_2O_3 sizes are all around 36–50 nm when the α-Al_2O_3 content is less than 5 wt%, regardless of the initial size of χ-Al_2O_3. The bright and dark-field TEM micrographs of C17 heated briefly at 1100 °C for 4 min, shown in Fig. 8(b), indicate that the system is composed of a large crystallite surrounded by numerous small crystallites of χ-Al_2O_3. The electron diffraction pattern illustrated in the inset confirms that the large crystallite is α-Al_2O_3 which already exhibits a size of around 40 nm.

Conclusively, Fig. 9 depicts a phase diagram as a function of particle size according to the present study. The particles of χ-Al_2O_3 larger than 40 nm have to be accomplished by two-step phase transformation, i.e. χ → κ → α-Al_2O_3. The temperature for the κ-Al_2O_3 formation increases with decreasing particle size due to the shape effect. However, it is easier for α-Al_2O_3 to transform from κ-Al_2O_3 due to the size effect. As the χ-Al_2O_3 particle size is below 40 nm, direct phase transformation χ → α-Al_2O_3 is dominant and occurs at 1050 °C without forming κ-Al_2O_3.

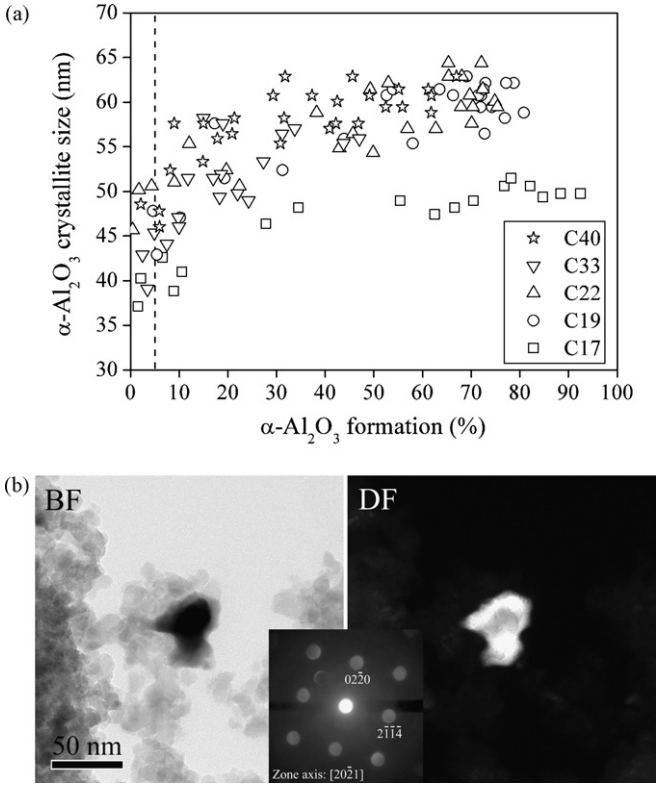

Fig. 8. (a) Crystallite size of α-Al_2O_3 as a function of its formation quantity of calcined C17, C19, C22, C33 and C40 χ-Al_2O_3 samples. (b) Bright and dark-field TEM images of α-Al_2O_3 crystallites directly transformed from C17 χ-Al_2O_3 samples holding at 1100 °C for 4 min, in which only χ- and α-Al_2O_3 crystallites were observed.

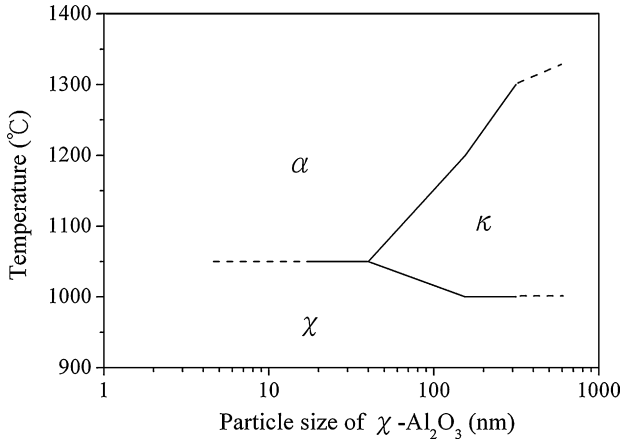

Fig. 9. Phase diagram related to the particle sizes of χ-Al_2O_3.

4. Conclusions

The present work describes shape and size effects on the phase transformation of χ-Al_2O_3 to α-Al_2O_3. It is found that $\chi \rightarrow \kappa$-Al_2O_3 transformation is strongly influenced by the particle shape. A complete platelet-like particle allows a transformation of $\chi \rightarrow \kappa$-Al_2O_3 occurs at 1000 °C which is obviously retarded when such platelet-like morphology is destroyed by fragment treatment. In addition, the temperature for the formation of α-Al_2O_3 is effectively lowered by reducing particle size. When the particle size decreases from 155 to 40 nm, the required activation energy is effectively decreased from 853 to 321 kJ/mol so that the formation of $\kappa \rightarrow \alpha$-$Al_2O_3$ reaction is thus lowered from 1300 to 1150 °C.

Furthermore, the critical size of χ-Al_2O_3 is determined to be around 40 nm. For the particle sizes larger than 40 nm, the phase transformation of χ-Al_2O_3 to α-Al_2O_3 must through κ-Al_2O_3. For those smaller than 40 nm, χ-Al_2O_3 can directly transform to α-Al_2O_3 bypassing κ-Al_2O_3. However, an initial crystal growth is necessary to reach such crystal size. This study confirms the importance of size effect on the phase transformation of χ-Al_2O_3 to κ-Al_2O_3. Reducing the particle size allows to the effective modification of the transition path and directly forms stable α-Al_2O_3 at low temperatures.

Acknowledgements

We thank Miss Liang-Chu Wang of National Sun Yat-Sen University for assistance in TEM examinations. This study was supported by the National Science Council, ROC under contract NSC-96-2221-E-006-122-MY2 and the Ministry of Economic Affairs, ROC under contract 96-EC-17-A-08-S1-023.

References

1. Gribb, A. A. and Banfield, J. F., Particle size effects on transformation kinetics and phase stability in nanocrystalline TiO_2. *Am. Mineral.*, 1997, **82**, 717–728.
2. Banfield, J. F. and Navrotsky, A.,*Reviews in Mineralogy and Geochemistry, Nanoparticles and the Environment*, *vol. 44*. The Mineralogical Society of America, Washington, DC, 2001, pp. 29–34.
3. Hsiang, H. I. and Yen, F. S., Effect of crystallite size on the ferroelectric domain growth of ultrafine $BaTiO_3$ powders. *J. Am. Ceram. Soc.*, 1996, **79**, 1053–1060.
4. Erdem, E., Semmelhack, H. C., Böttcher, R., Rumpf, H., Banys, J., Matthes, A. *et al.*, Study of the tetragonal-to-cubic phase transformation in $PbTiO_3$ nanopowders. *J. Phys.: Condens. Matter*, 2006, **18**, 3874–3961.
5. Zhang, Y. L., Jin, X. J., Rong, Y. H., Hsu, T. Y., Jiang, D. Y. and Shi, J. L., The size dependence of structural stability in nano-sized ZrO_2 particles. *Mater. Sci. Eng. A*, 2006, **438–440**, 399–402.
6. Garvie, R. C., Occurrence of metastable tetragonal zirconia as a crystallite size effect. *J. Phys. Chem.*, 1965, **69**, 1238–1243.
7. Kingery, W. D., Bowen, H. K. and Uhlmann, D. R., *Introduction to Ceramics* (*2nd ed.*). John Wiley & Sons, New York, 1975, pp. 328–346.
8. Putnis, A. and McConnell, J. D. C.,*Geoscience Texts: Principles of Mineral Behaviour*, *vol. 1*. Elsevier, New York, 1980.
9. Wen, H. L. and Yen, F. S., Growth characteristics of boehmite-derived ultrafine theta and alpha-alumina particles during phase transformation. *J. Cryst. Growth*, 2000, **208**, 696–708.
10. Chang, P. L., Yen, F. S., Cheng, K. C. and Wen, H. L., Examinations on the critical and primary crystallite sizes during θ- to α-phase transformation of ultrafine alumina powders. *Nano Lett.*, 2001, **1**, 253–261.
11. Zhang, H. and Banfield, J. F., New kinetic model for the nanocrystalline anatase-to-rutile transformation revealing rate dependence on number of particles. *Am. Mineral.*, 1999, **84**, 528–535.
12. Brindley, G. W. and Choe, J. O., The reaction series, gibbsite → chi alumina → kappa alumina → corundum. *Am. Mineral.*, 1961, **46**, 771–785.
13. Wefers, K. and Bell, G. M., *Oxides and Hydroxides of Alumina*. Alcoa Research Laboratories, 1972, Technical Paper No. 19.
14. Inoue, M., Kominami, H. and Inui, T., Thermal transformation of χ-alumina formed by thermal decomposition of aluminum alkoxide in organic media. *J. Am. Ceram. Soc.*, 1992, **75**, 2597–2598.
15. Mekasuwandumrong, O., Silveston, P. L., Praserthdam, P., Inoue, M., Pavarajarn, V. and Tanakulrungsank, W., Synthesis of thermally stable micro spherical χ-alumina by thermal decomposition of alumium isopropoxide in mineral oil. *Inorg. Chem. Commun.*, 2003, **6**, 930–934.
16. Mekasuwandumrong, O., Praserthdam, P., Inoue, M., Pavarajarn, V. and Tanakulrungsank, W., Phase transformation behavior of nanocrystalline χ-alumina powder obtained by thermal decomposition of AIP in inert organic solvent. *J. Mater. Sci.*, 2004, **39**, 2417–2421.
17. MacKenzie, K. J. D., Temuujin, J., Smith, M. E., Angerer, P. and Kameshima, Y., Effect of mechanochemical activation on the thermal reactions of boehmite (γ-AlOOH) and γ-Al_2O_3. *Thermochim. Acta*, 2000, **359**, 87–94.
18. Kano, J., Saeki, S., Saito, F., Tanjo, M. and Yamazaki, S., Application of dry grinding to reduction in transformation temperature of aluminum hydroxides. *Int. J. Miner. Process.*, 2000, **60**, 91–100.
19. Torres Sánchez, R. M., Boix, A. and Mercader, R. C., Grinding assistance in the transformation of gibbsite to corundum. *J. Mater. Res.*, 2002, **17**, 712–717.
20. Chang, P. L. *Particle size effects on gibbsite to α-Al_2O_3 phase transformation*. PhD Thesis. National Cheng Kung Univ., Taiwan, ROC, 2008.
21. Cullity, B. D., *Elements of X-Ray Diffraction* (*2nd ed.*). Addison-Wesley, London, 1978.
22. Punis, A., *Introduction to Mineral Sciences*. Cambridge Univ. Press, 1992.
23. Ollivier, B., Retoux, R., Lacorre, P., Massiot, D. and Férey, G., Crystal structure of κ-alumina: an X-ray powder diffraction, TEM and NMR study. *J. Mater. Chem.*, 1997, **7**, 1049–1056.
24. Santos, H. S., Campos, T. W., Santos, P. S. and Kiyohara, P. K., Thermal Phase sequences in gibbsite/kaolinite clay: electron microscopy studies. *Ceram. Int.*, 2005, **31**, 1077–1084.
25. Christian, J. W., *The Theory of Transformations in Metals and Alloys*. Pergamon Press, New York, 1965.